Renormalized cluster expansion of the microfield distribution in a strongly coupled two-component plasmas

H.B.Nersisyan* and D.A.Osipyan
Division of Theoretical Physics, Institute of Radiophysics and Electronics, Alikhanian Brothers str.1, 378410 Ashtarak, Armenia

G.Zwicknagel†
Institut für Theoretische Physik II, Erlangen-Nürnberg Universität, Staudtstrasse 7, D-91058 Erlangen, Germany
(Dated: February 2, 2008)

The electric microfield distribution (MFD) at an impurity ion is studied for two-component (TCP) electron-ion plasmas using molecular dynamics simulation and theoretical models. The particles are treated within classical statistical mechanics using an electron-ion Coulomb potential regularized at distances less than the de Broglie length to take into account quantum-diffraction effects. Corrections to the potential-of-mean-force exponential (PMFEX) approximation recently proposed for MFD in a strongly coupled TCP [Phys. Rev. E **72**, 036403 (2005)] are obtained and discussed. This has been done by a generalization of the standard Baranger-Mozer and renormalized cluster expansion techniques originally developed for the one-component plasmas to the TCPs. The results obtained for a neutral point are compared with those from molecular dynamics simulations. It is shown that the corrections do not help to improve the PMFEX approximation for a TCP with low ionic charge Z. But starting with $Z > 5$ the PMFEX model is substantially improved and the agreement with numerical simulations is excellent. We have also found that with increasing coupling the PMFEX approximation becomes invalid to predict the MFD at a neutral point while its corrected version agrees satisfactory with the simulations.

PACS numbers: 52.27.Gr, 52.27.Aj, 52.65.Yy, 05.10.-a

I. INTRODUCTION

The determination of the electric microfield distribution at a neutral atom or charged impurity ion (radiator) in a plasma is an important tool for the understanding of many spectroscopic experiments [1, 2]. Since the pioneering work of Holtsmark [3], who completely neglected correlations between the particles (ideal plasma), many efforts have been concentrated on an improved statistical description of the microfield distribution. The first theory which goes beyond the Holtsmark limit and which is based on a cluster expansion similar to that of Ursell and Mayer [4] was developed by Baranger and Mozer [5, 6]. In this approach the microfield distribution is represented as an expansion in terms of correlation functions which has been truncated on the level of the pair correlation. The latter is treated in the Debye-Hückel form which corresponds to the first order of the expansion in the coupling parameter. The theory by Baranger and Mozer was improved by Hooper [7, 8]. They reformulated the expansion of the microfield distribution in terms of other functions by introducing a free parameter which was adjusted in such a way to arrive at a level where the resulting microfield distribution did not depend on the free parameter any more. However, it was argued that such a method is only valid at small coupling parameters, where the correction to the Holtsmark distribution, corresponding to the first term in the series, is small. The first theory capable to provide reliable numerical results for strongly coupled plasmas, known as adjustable-parameter exponential approximation (APEX), was proposed by Iglesias and co-workers [9, 10]. It involves a noninteracting quasiparticle representation of the electron-screened ions. This phenomenological but highly successful approximation is based on a parameterization of the electric microfield produced on a radiator with the Debye-Hückel-type screened interaction with unknown screening length. This free parameter is then adjusted in such a way to yield the correct second moment of the microfield distribution. Afterwards the APEX model was substantially improved for neutral radiators using renormalized correlation functions and electric fields [11]. (We refer the reader to Ref. [12] for a recent review).

Most of this work was done on one-component plasmas (OCP) and thus neglects the influence of the attractive interactions between electrons and ions. In this paper we study the microfield distribution in a two-component

*Electronic address: hrachya@irphe.am
†Electronic address: zwicknagel@theorie2.physik.uni-erlangen.de

plasmas (TCP). This has been done previously in Refs. [13, 14] for partially degenerate electrons. In Ref. [13] the low-frequency component of the microfield was calculated within the linear response treatment taking strong correlations into account via local field corrections. Also the problem of attractive interaction has been considered for a single but highly charged impurity ion immersed in an electronic OCP [15]. In the recent papers [16, 17] we already studied strongly coupled systems, i.e., a highly charged radiator in a TCP of classical (nondegenerated) and strongly correlated particles beyond a perturbative treatment. As in Ref. [13] the theoretical scheme (PMFEX) presented in Refs. [16, 17] is based on the potential-of-mean-force approximation. It exactly satisfies the sum-rule requirement arising from the second moment of the microfield distribution without introducing adjustable parameters. Comparisons of the PMFEX calculations with the molecular-dynamics simulations for the electric fields at the highly charged points relevant for laser-produced plasmas show, in general, an excellent agreement even for large coupling [16]. However, the results of the PMFEX for neutral points have not yet been comprehensively tested. Here, the PMFEX scheme may be less accurate [17], similar as it occurs in the APEX where further improvement for microfield distribution at neutral point is needed, see Ref. [11]. Moreover, in a regime dominated by small local fields and hence by small local electronic density the PMFEX deviates from the molecular-dynamics simulations also for charged radiator [16]. This feature has been clearly observed for a single ion embedded in an electronic OCP in Ref. [15]. Therefore, it is of interest to improve the PMFEX model and provide a tool for calculating the corrections to it when required. Our purpose here is to introduce the key ideas of PMFEX in the standard Baranger-Mozer cluster representation for the microfield distributions [5, 6]. In this way some contact between PMFEX and standard small plasma-parameter theories is established, while also providing PMFEX as the leading term in a series from which corrections can be calculated explicitly. Another important ingredient of our treatment is the electron-ion attractive interaction which drastically changes the physical properties of the system as compared to classical OCPs (see, e.g., Ref. [15]). But the thermodynamic stability of a TCP requires at least some quantum features for the electron-ion interaction at short distances. This required minimum of quantum features is here taken into account by using a regularized ion-electron potential [18, 19, 20], which then enables the application of classical statistical mechanics and classical MD simulations.

The paper is organized as follows. In Sec. II, we define the basic parameters of interest for a TCP. The theoretical schemes applied previously to either electronic or ionic OCPs are generalized to TCPs in Secs. III and IV. In particular, starting with the canonical ensemble formulation of the microfield distribution in the TCP the Baranger-Mozer treatment is reviewed and the structure of the resulting cluster series is discussed in Sec. III. Next, the basic assumptions of the PMFEX are briefly given and motivated in Sec. IV. Here a formal relationship of the PMFEX to the Baranger-Mozer series is established and the first two terms of a renormalized cluster series are given explicitly. Furthermore, to test obtained theoretical results in Sec. V the correction terms are calculated at a neutral point and compared with the results from classical molecular dynamics simulations. The results are summarized in Sec. VI. The exact second moment of the microfield distribution at a neutral point is considered in the Appendix A.

II. BASIC PARAMETERS FOR THE TCP

We consider a neutral and isotropic two-component electron-ion plasma consisting of ions and electrons at a temperature T in a volume Ω. The particles are assumed to be classical and pointlike. The average densities, charges, and masses of the ions and electrons are n_i, n_e, and Ze, $-e$ and m_i, m, respectively. We assume that the density of radiator ions or atoms are small, $n_R \ll n_{i;e}$ and thus consider only one radiator ion with charge $Z_R e$ in our calculations (throughout this paper the index R refers to the radiators). Because of the charge neutrality we have $n_e = n_i Z$.

We now introduce the Coulomb coupling parameters $\Gamma_{\alpha\beta}$. Introducing the Wigner-Seitz radii, i.e., the mean electron-electron, electron-ion, and ion-ion distances through the relations, $a_e^{-3} = 4\pi n_e/3$, $a^{-3} = 4\pi n/3$, and $a_i^{-3} = 4\pi n_i/3$ (where $n = n_e + n_i$ is the plasma total density) these parameters are defined as

$$\Gamma_{ee} = \frac{e_S^2}{a_e k_B T}, \quad \Gamma_{ei} = \frac{Z e_S^2}{a k_B T}, \quad \Gamma_{ii} = \frac{Z^2 e_S^2}{a_i k_B T}, \tag{1}$$

respectively, where $e_S^2 = e^2/4\pi\varepsilon_0$. Note that

$$\Gamma_{ee} = \frac{\Gamma_{ei}}{\left[Z^2\,(Z+1)\right]^{1/3}}, \quad \Gamma_{ii} = \frac{Z\Gamma_{ei}}{(Z+1)^{1/3}}. \tag{2}$$

In a hydrogen plasma with $Z = 1$ we obtain $\Gamma_{ee} = \Gamma_{ii} = 2^{-1/3}\Gamma_{ei}$ while in a plasma with highly charged ions ($Z \gg 1$) $\Gamma_{ii} = Z^{2/3}\Gamma_{ei} \gg \Gamma_{ee} = \Gamma_{ei}/Z$. So, in the TCP with uncorrelated electrons the ions may be strongly correlated.

The Holtsmark field E_H for a TCP is given by $E_H^{3/2} = E_{He}^{3/2} + E_{Hi}^{3/2}$ (see Ref. [16] for details), where E_{He} and E_{Hi} are the electronic and ionic Holtsmark fields, respectively, $E_{He} = Ce_F/a_e^2$, $E_{Hi} = CZe_F/a_i^2$ with $C = (8\pi/25)^{1/3}$ and

$e_F = e/4\pi\varepsilon_0$. Since $E_{He} = Z^{-1/3}E_{Hi}$ the electronic and ionic components of a hydrogen TCP contribute equally to the Holtsmark field. For a completely ionized TCP with highly charged ions the ions dominate E_H. The definition of the Holtsmark field E_H for a TCP is equivalent to the obvious relation $n = n_e + n_i$ and can be represented as

$$E_H = \frac{C\mathcal{Z}e_F}{a^2}, \qquad \mathcal{Z} = \left[\frac{Z\left(1+Z^{1/2}\right)}{(Z+1)}\right]^{2/3} \tag{3}$$

with an effective charge $\mathcal{Z}$.

For the regularized pair interaction potential $e_S^2 q_\alpha q_\beta u_{\alpha\beta}(r)$ with $\alpha, \beta = e, i, R$, $q_e = -1$, $q_i = Z$, $q_R = Z_R$, we here employ

$$u_{\alpha\beta}(r) = \frac{1}{r}\left(1 - e^{-r/\delta_{\alpha\beta}}\right). \tag{4}$$

The cutoff parameters $\delta_{\alpha\beta}$ are related to the thermal de Broglie wavelengths, $\delta_{\alpha\beta} = \left(\hbar^2/\mu_{\alpha\beta}k_BT\right)^{1/2}$, where $\mu_{\alpha\beta}$ is the reduced mass of the particles α and β. For large distances $r > \delta_{\alpha\beta}$ the potential becomes Coulomb, while for $r < \delta_{\alpha\beta}$ the Coulomb singularity is removed and $u_{\alpha\beta}(0) = 1/\delta_{\alpha\beta}$. By this the short range effects based on the uncertainty principle are included [18, 19, 20]. We point out that the dependence on the physical parameters density and temperature is implicitly contained in the parameters $\Gamma_{\alpha\beta}$ and $\delta_{\alpha\beta}$.

III. GENERALIZATION OF THE BARANGER-MOZER FORMULATION TO THE TCP

A. Preliminaries

The electric microfield distribution (MFD) $Q(\mathbf{E})$ is defined as the probability density of finding a field $\mathbf{E}$ at a charge Z_Re, located at $\mathbf{r}_0$, in a TCP with N_i ions and N_e electrons. This system is described by classical statistical mechanics in a canonical ensemble of $(N_i + N_e + 1)$ particles, and temperature T. The normalized probability density of the microfield $\mathbf{E}$ is then given by [13, 16]

$$Q(\mathbf{E}) = \frac{1}{W}\int_\Omega e^{-\beta_T U(\mathcal{T}_e,\mathcal{T}_i,\mathbf{r}_0)}\delta\left(\mathbf{E} - \mathbf{E}\left(\mathcal{T}_e,\mathcal{T}_i,\mathbf{r}_0\right)\right)d\mathbf{r}_0 d\mathcal{T}_e d\mathcal{T}_i, \tag{5}$$

where $\beta_T = 1/k_BT$, and $\mathcal{T}_e = \{\mathbf{r}_1, \mathbf{r}_2 ... \mathbf{r}_{N_e}\}$, $\mathcal{T}_i = \{\mathbf{R}_1, \mathbf{R}_2 ... \mathbf{R}_{N_i}\}$ are the coordinates of electrons and ions, respectively, and

$$W = \int_\Omega e^{-\beta_T U(\mathcal{T}_e,\mathcal{T}_i,\mathbf{r}_0)}d\mathbf{r}_0 d\mathcal{T}_e d\mathcal{T}_i \tag{6}$$

is the canonical partition function. $U(\mathcal{T}_e, \mathcal{T}_i, \mathbf{r}_0)$ is the potential energy of the configuration given here by

$$U(\mathcal{T}_e,\mathcal{T}_i,\mathbf{r}_0) = e_S^2\left[\frac{1}{2}\sum_{\alpha,\beta,a,b} q_\alpha q_\beta u_{\alpha\beta}(|\mathbf{r}_a^{(\alpha)} - \mathbf{r}_b^{(\beta)}|) + Z_R\sum_{\alpha,a} q_\alpha u_{\alpha R}(|\mathbf{r}_0 - \mathbf{r}_a^{(\alpha)}|)\right] \tag{7}$$

in terms of the pair interaction potentials $u_{\alpha\beta}(r)$ and $u_{\alpha R}(r)$, where $\alpha, \beta = e, i$, $\mathbf{r}_a^{(e)} = \mathbf{r}_a$, $\mathbf{r}_a^{(i)} = \mathbf{R}_a$. In Eq. (7) the first sum is restricted to $a \neq b$ for identical particles, $\alpha = \beta$. The total electrical field $\mathbf{E}(\mathcal{T}_e, \mathcal{T}_i, \mathbf{r}_0)$ acting on the radiator is given by the superposition of electronic and ionic single-particle fields

$$\mathbf{E}(\mathcal{T}_e,\mathcal{T}_i,\mathbf{r}_0) = -\frac{1}{Z_Re}\nabla_0 U = \sum_{a=1}^{N_e}\mathbf{E}_e(\mathbf{r}_0 - \mathbf{r}_a) + \sum_{a=1}^{N_i}\mathbf{E}_i(\mathbf{r}_0 - \mathbf{R}_a). \tag{8}$$

As $\mathbf{E}_\alpha(\mathbf{r}) = \frac{\mathbf{r}}{r}E_\alpha(r)$, we obtain for the electronic and ionic single-particle fields $E_e(r) = e_F u'_{eR}(r)$, $E_i(r) = -Ze_F u'_{iR}(r)$, where the prime indicates derivative with respect to r.

The spherical symmetric interaction between plasma particles and the isotropy of the system allows to introduce the normalized microfield distribution $P(E) = 4\pi E^2 Q(E)$. It can be reexpressed in terms of the Fourier transform of $Q(E)$ through

$$P(E) = \frac{2E^2}{\pi}\int_0^\infty T(\kappa)\, j_0(\kappa E)\,\kappa^2 d\kappa, \quad T(\kappa) = \int_0^\infty P(E)\, j_0(\kappa E)\, dE, \tag{9}$$

and

$$T(\boldsymbol{\kappa}) = \left\langle e^{i\boldsymbol{\kappa}\cdot\mathbf{E}} \right\rangle = \frac{1}{W}\int_{\Omega} \exp\left[i\boldsymbol{\kappa}\cdot\mathbf{E}\left(\mathcal{T}_e,\mathcal{T}_i,\mathbf{r}_0\right)\right] e^{-\beta_T U(\mathcal{T}_e,\mathcal{T}_i,\mathbf{r}_0)} d\mathbf{r}_0 d\mathcal{T}_e d\mathcal{T}_i, \tag{10}$$

where $\langle ... \rangle$ denotes a statistical average and $j_0(x) = \sin x/x$ is the spherical Bessel function of order zero. The coefficients of the expansion of the function $T(\kappa)$ at $\kappa \to 0$ yield the even moments of the microfield distribution,

$$T(\kappa) = 1 - \frac{\kappa^2}{6}\left\langle E^2 \right\rangle + \frac{\kappa^4}{120}\left\langle E^4 \right\rangle - ... \tag{11}$$

The similar expansion for the function $\mathcal{L}(\kappa)$ defined by $T(\kappa) = e^{-\mathcal{L}(\kappa)}$ yields

$$\mathcal{L}(\kappa) = \frac{\kappa^2}{6}\left\langle E^2 \right\rangle + \frac{\kappa^4}{72}\left[\left\langle E^2 \right\rangle^2 - \frac{3}{5}\left\langle E^4 \right\rangle\right] + ... \tag{12}$$

Therefore the Fourier transform of the MFD can be interpreted as a generating function for microfield even moments. Equations (5)-(12) describe the total MFD at the position $\mathbf{r}_0$ of the radiator generated by both the statistically distributed ions and electrons of the TCP. Since we are interested to calculate the MFD, Eq. (9), in an infinite system the statistical average of any quantity becomes translationally invariant with respect to $\mathbf{r}_0$, and the location of the test charge may be taken as the origin without loss of generality.

B. Baranger-Mozer cluster expansion for the TCP

In this section we generalize the Baranger-Mozer (BM) cluster expansion technique originally developed for one-component plasmas (see, e.g., [5, 6, 7, 8]) to the classical TCPs. This method results from two transformations of Eq. (5). The first is motivated by the fact that the required average in Eq. (10) is the product of electronic and ionic single-particle functions, $e^{i\boldsymbol{\kappa}\cdot\mathbf{E}_e(\mathbf{r}_a)}$ and $e^{i\boldsymbol{\kappa}\cdot\mathbf{E}_i(\mathbf{R}_a)}$, which have a value close to one over some volume of the system. This suggest a first transformation to the set of single-particle functions

$$\chi_a^{(\alpha)}(\boldsymbol{\kappa}) = e^{i\boldsymbol{\kappa}\cdot\mathbf{E}_\alpha\left(\mathbf{r}_a^{(\alpha)}\right)} - 1. \tag{13}$$

Using this transformation the exponential factor in Eq. (10) becomes (for simplicity we drop the coordinate $\mathbf{r}_0$ of the radiator)

$$\exp\left[i\boldsymbol{\kappa}\cdot\mathbf{E}\left(\mathcal{T}_e,\mathcal{T}_i\right)\right] = \prod_{a=1}^{N_e}\left[1+\chi_a^{(e)}(\boldsymbol{\kappa})\right]\prod_{b=1}^{N_i}\left[1+\chi_b^{(i)}(\boldsymbol{\kappa})\right]. \tag{14}$$

The introduced single-particle functions $\chi_a^{(\alpha)}$ have the advantage to be zero over some volume. The spirit of this transformation to the functions $\chi_a^{(\alpha)}$ is similar to the use of Mayer's f-functions for thermodynamic properties of gases [4]. Substituting Eq. (14) into Eq. (10) leads in the thermodynamic limit directly to the series

$$\begin{aligned} T(\boldsymbol{\kappa}) \;=\; & 1 + \sum_{\alpha}\sum_{a=1}^{\infty}\frac{n_\alpha^a}{a!}\int \chi_1^{(\alpha)}(\boldsymbol{\kappa})\,\chi_2^{(\alpha)}(\boldsymbol{\kappa})...\chi_a^{(\alpha)}(\boldsymbol{\kappa})\,\mathcal{G}_a^{(\alpha)}(\mathcal{T}_a^{(\alpha)})d\mathcal{T}_a^{(\alpha)} \\ & + \sum_{a=1}^{\infty}\frac{n_e^a}{a!}\sum_{b=1}^{\infty}\frac{n_i^b}{b!}\int \chi_1^{(e)}(\boldsymbol{\kappa})...\chi_a^{(e)}(\boldsymbol{\kappa})\,\chi_1^{(i)}(\boldsymbol{\kappa})...\chi_b^{(i)}(\boldsymbol{\kappa})\,\mathcal{G}_{ab}^{(ei)}(\mathcal{T}_a^{(e)},\mathcal{T}_b^{(i)})d\mathcal{T}_a^{(e)}d\mathcal{T}_b^{(i)}, \end{aligned} \tag{15}$$

where $\mathcal{T}_a^{(\alpha)} = \{\mathbf{r}_1^{(\alpha)},\mathbf{r}_2^{(\alpha)},...\mathbf{r}_a^{(\alpha)}\}$ and $d\mathcal{T}_a^{(\alpha)} = d\mathbf{r}_1^{(\alpha)}d\mathbf{r}_2^{(\alpha)}...d\mathbf{r}_a^{(\alpha)}$. Here $\mathcal{G}_a^{(\alpha)}(\mathcal{T}_a^{(\alpha)})$ and $\mathcal{G}_{ab}^{(ei)}(\mathcal{T}_a^{(e)},\mathcal{T}_b^{(i)})$ are equilibrium correlation functions. The first quantity represents the probability density for a particles from plasma species α at $\mathbf{r}_1^{(\alpha)}$, $\mathbf{r}_2^{(\alpha)}$,...$\mathbf{r}_a^{(\alpha)}$, and the test particle at the origin. The second one describes the correlations between a electrons at $\mathbf{r}_1$, $\mathbf{r}_2$,...$\mathbf{r}_a$, and b ions at $\mathbf{R}_1$, $\mathbf{R}_2$,...$\mathbf{R}_b$ involving the test particle. The range of integration for each term in Eq. (15) is now restricted by the $\chi_a^{(\alpha)}(\boldsymbol{\kappa})$-functions. However, this restriction is not uniform with respect to $\boldsymbol{\kappa}$, and particularly for large values of $\boldsymbol{\kappa}$ the functions $\chi_a^{(\alpha)}(\boldsymbol{\kappa})$ can differ from zero over a correspondingly large volume. Consequently, a second transformation is desirable, $T(\boldsymbol{\kappa}) = e^{-\mathcal{L}(\boldsymbol{\kappa})}$, where by a standard theorem of equilibrium statistical mechanics (see, e.g., [21]), $\mathcal{L}(\boldsymbol{\kappa})$ is determined from Eq. (15) as

$$\mathcal{L}(\boldsymbol{\kappa}) = -\sum_{\alpha}\sum_{a=1}^{\infty}\frac{n_\alpha^a}{a!}h_a^{(\alpha)}(\boldsymbol{\kappa}) - \sum_{a=1}^{\infty}\frac{n_e^a}{a!}\sum_{b=1}^{\infty}\frac{n_i^b}{b!}h_{ab}^{(ei)}(\boldsymbol{\kappa}). \tag{16}$$

Here $h_a^{(\alpha)}(\boldsymbol{\kappa})$ and $h_{ab}^{(ei)}(\boldsymbol{\kappa})$ are given by

$$h_a^{(\alpha)}(\boldsymbol{\kappa}) = \int \chi_1^{(\alpha)}(\boldsymbol{\kappa})\,\chi_2^{(\alpha)}(\boldsymbol{\kappa})\ldots\chi_a^{(\alpha)}(\boldsymbol{\kappa})\,\ell_a^{(\alpha)}(\mathcal{T}_a^{(\alpha)})d\mathcal{T}_a^{(\alpha)}, \tag{17}$$

$$h_{ab}^{(ei)}(\boldsymbol{\kappa}) = \int \chi_1^{(e)}(\boldsymbol{\kappa})\ldots\chi_a^{(e)}(\boldsymbol{\kappa})\,\chi_1^{(i)}(\boldsymbol{\kappa})\ldots\chi_b^{(i)}(\boldsymbol{\kappa})\,\ell_{ab}^{(ei)}(\mathcal{T}_a^{(e)},\mathcal{T}_b^{(i)})d\mathcal{T}_a^{(e)}d\mathcal{T}_b^{(i)}, \tag{18}$$

and $\ell_a^{(\alpha)}$ and $\ell_{ab}^{(ei)}$ are the Ursell cluster functions for TCP associated with the set of usual correlation functions $\mathcal{G}_a^{(\alpha)}$ and $\mathcal{G}_{ab}^{(ei)}$, respectively. The functions $\ell_a^{(\alpha)}$ for electron-electron and ion-ion interactions are expressed by the correlation functions $\mathcal{G}_a^{(\alpha)}$ in the same manner as in the case of corresponding OCP (see, e.g., [5, 6, 7]). Therefore, as an example we consider here explicitly only the functions $\ell_{ab}^{(ei)}$ which involve electron-ion interactions,

$$\ell_{11}^{(ei)}(\mathbf{r}_1,\mathbf{R}_1) = \mathcal{G}_{11}^{(ei)}(\mathbf{r}_1,\mathbf{R}_1) - \mathcal{G}_1^{(e)}(\mathbf{r}_1)\,\mathcal{G}_1^{(i)}(\mathbf{R}_1), \tag{19}$$

$$\begin{aligned}\ell_{12}^{(ei)}(\mathbf{r}_1,\mathbf{R}_1,\mathbf{R}_2) \;=\; & \mathcal{G}_{12}^{(ei)}(\mathbf{r}_1,\mathbf{R}_1,\mathbf{R}_2) - \mathcal{G}_1^{(e)}(\mathbf{r}_1)\,\mathcal{G}_2^{(i)}(\mathbf{R}_1,\mathbf{R}_2) - \mathcal{G}_1^{(i)}(\mathbf{R}_1)\,\mathcal{G}_{11}^{(ei)}(\mathbf{r}_1,\mathbf{R}_2) \\ & -\mathcal{G}_1^{(i)}(\mathbf{R}_2)\,\mathcal{G}_{11}^{(ei)}(\mathbf{r}_1,\mathbf{R}_1) + 2\mathcal{G}_1^{(e)}(\mathbf{r}_1)\,\mathcal{G}_1^{(i)}(\mathbf{R}_1)\,\mathcal{G}_1^{(i)}(\mathbf{R}_2),\end{aligned} \tag{20}$$

$$\begin{aligned}\ell_{21}^{(ei)}(\mathbf{r}_1,\mathbf{r}_2,\mathbf{R}_1) \;=\; & \mathcal{G}_{21}^{(ei)}(\mathbf{r}_1,\mathbf{r}_2,\mathbf{R}_1) - \mathcal{G}_1^{(i)}(\mathbf{R}_1)\,\mathcal{G}_2^{(e)}(\mathbf{r}_1,\mathbf{r}_2) - \mathcal{G}_1^{(e)}(\mathbf{r}_1)\,\mathcal{G}_{11}^{(ei)}(\mathbf{r}_2,\mathbf{R}_1) \\ & -\mathcal{G}_1^{(e)}(\mathbf{r}_2)\,\mathcal{G}_{11}^{(ei)}(\mathbf{r}_1,\mathbf{R}_1) + 2\mathcal{G}_1^{(e)}(\mathbf{r}_1)\,\mathcal{G}_1^{(e)}(\mathbf{r}_2)\,\mathcal{G}_1^{(i)}(\mathbf{R}_1)\end{aligned} \tag{21}$$

etc., for pair and three-body correlations, respectively. The higher order Ursell functions involving $\geqslant 4$ particles can be constructed similarly. All single-particle Ursell functions are here expressed by the ordinary pair correlation function between radiator and plasma particles of species α, $\ell_1^{(\alpha)}(\mathbf{r}) = \mathcal{G}_1^{(\alpha)}(\mathbf{r}) = g_{\alpha R}(r)$ [16]. The significant difference between $\mathcal{G}$ and ℓ correlation functions is that the cluster functions ℓ vanish when any members of the particles are sufficiently far apart, whereas the ordinary correlation functions $\mathcal{G}$ have not this property. In particular, for completely uncorrelated system of particles the many-body functions $\mathcal{G}$ tend to unity while $\ell \to 0$ beginning with $\ell_{11}^{(ei)}$ and $\ell_2^{(\alpha)}$. Hence, the range of the integrals in Eq. (16) is controlled by both the functions $\chi_a^{(\alpha)}(\boldsymbol{\kappa})$ and the Ursell functions. The later restricts the integration to volumes characterized by the correlation length which depends on the thermodynamic-state condition but is independent of $\boldsymbol{\kappa}$. Qualitatively, therefore, the BM formalism provides a series representation whose terms are controlled by the range of $\chi_a^{(\alpha)}(\boldsymbol{\kappa})$ for small $\boldsymbol{\kappa}$ and by the range of the Ursell functions for large $\boldsymbol{\kappa}$.

Equations (16)-(18) together with the relation $T(\boldsymbol{\kappa}) = e^{-\mathcal{L}(\boldsymbol{\kappa})}$ constitutes the generalization of the Baranger-Mozer cluster expansion technique to the TCPs. In contrast to the BM theory developed for OCP Eq. (16) now involves terms which are responsible for electron-electron, ion-ion and electron-ion attractive interactions. The BM result is easily recovered from Eq. (16) by neglecting the last term as well as one of two terms responsible for the interactions between identical particles. In addition, for ideal TCPs (Holtsmark limit) the second sum in Eq. (16) and all terms with $a \geqslant 2$ in the first sum vanish, and only the term with $a = 1$ in the first sum contributes to the MFD. It is easy to see that this term coincides with the result of Ref. [16] derived for ideal TCP.

From a practical point of view, it is too difficult to calculate correlation functions of higher order than $\mathcal{G}_2^{(\alpha)}$ and $\mathcal{G}_{11}^{(ei)}$. For weakly coupled plasmas, the Ursell functions of order $\lambda+1$ are typically of the order of the plasma parameters to the power λ. Therefore Eq. (16) is usually truncated at first, second or in some cases at third order. If the correlation functions are expanded as well with respect to the plasma parameters and truncated at the corresponding order the MFD with Eqs. (16)-(18) can be evaluated analytically (see, e.g., Refs. [5, 6, 7, 8, 22, 23]). Obviously, such a method may be successful only for weakly coupled plasmas. A possible extension to the strongly coupled regimes requires that the BM representation sufficiently rapidly converges to allow for a truncation after the first two terms. This suggests, for instance, that the BM series could be improved if the bare single-particle electric fields in the χ-functions are replaced by screened fields representing the effects of strong correlations in a plasma. The formal procedure for carrying out such a "renormalization" has been developed in Ref. [24] and has been previously employed for OCPs [11]. In the next Sec. IV we extend this renormalization procedure to the two-component plasmas.

IV. RENORMALIZATION OF THE BARANGER-MOZER CLUSTER SERIES

A. PMFEX as independent-particle model

In Refs. [16, 17] we introduced the potential of mean force exponential approximation (PMFEX) which links the MFD to the pair correlation functions. To make further progress we briefly outline here the basic concepts of the PMFEX approximation. We show that similarly to the APEX (see, e.g., [9, 10, 11]) PMFEX is also an effective independent-particle model. Based on this assumption the MFD within PMFEX is derived quite simply. If all interactions between the plasma particles, except those with the radiator, are neglected, then the Ursell functions $\ell_a^{(\alpha)}$ vanish for $a \geqslant 2$ and $\ell_{ab}^{(ei)}(\mathcal{T}_a^{(e)}, \mathcal{T}_b^{(i)}) = 0$ for arbitrary a and b. The BM series (16) then reduces to only the leading term,

$$\mathcal{L}^{(0)}(\boldsymbol{\kappa}) = -\sum_\alpha n_\alpha \int \chi_1^{(\alpha)}(\boldsymbol{\kappa})\, g_{\alpha R}^{(0)}(\mathbf{r}_1)\, d\mathbf{r}_1. \tag{22}$$

The superscript (0) denotes the corresponding quantity without interactions among plasma particles. The PMFEX approach retains the independent-particle form of (22),

$$\mathcal{L}^{(0)}(\boldsymbol{\kappa}) \to \mathcal{L}(\boldsymbol{\kappa}) = -\sum_\alpha n_\alpha \int \psi_1^{(\alpha)}(\boldsymbol{\kappa})\, g_{\alpha R}^{*}(\mathbf{r}_1)\, d\mathbf{r}_1, \tag{23}$$

with the assumption that the important effects of correlations can be accounted for by an effective pair distribution function $g_{\alpha R}^{*}(\mathbf{r}_1)$ and a screened field $\boldsymbol{\mathcal{E}}_\alpha(\mathbf{r}_1)$ replacing the single-particle field $\mathbf{E}_\alpha(\mathbf{r}_1)$ in $\chi_1^{(\alpha)}(\boldsymbol{\kappa})$,

$$\psi_1^{(\alpha)}(\boldsymbol{\kappa}) = e^{i\boldsymbol{\kappa}\cdot\boldsymbol{\mathcal{E}}_\alpha(\mathbf{r}_1)} - 1. \tag{24}$$

Some constraint must be imposed to determine $g_{\alpha R}^{*}(\mathbf{r}_1)$. As in the case of APEX [9] this is a requirement that the effective "quasiparticle" field due to the effective charge density at $\mathbf{r}_1$ is equal to the corresponding exact field

$$g_{\alpha R}^{*}(\mathbf{r}_1)\, \boldsymbol{\mathcal{E}}_\alpha(\mathbf{r}_1) = g_{\alpha R}(\mathbf{r}_1)\, \mathbf{E}_\alpha(\mathbf{r}_1). \tag{25}$$

Assuming the spherical symmetric interactions with $\boldsymbol{\mathcal{E}}_\alpha(\mathbf{r}) = \frac{\mathbf{r}}{r}\mathcal{E}_\alpha(r)$ and $\mathbf{E}_\alpha(\mathbf{r}) = \frac{\mathbf{r}}{r}E_\alpha(r)$, this condition then define the PMFEX model as

$$\mathcal{L}_{\mathrm{PMFEX}}(\kappa) = \sum_\alpha 4\pi n_\alpha \int_0^\infty E_\alpha(r)\, \frac{1 - j_0(\kappa\mathcal{E}_\alpha(r))}{\mathcal{E}_\alpha(r)} g_{\alpha R}(r)\, r^2 dr. \tag{26}$$

In practice $g_{\alpha R}(r)$ is calculated from the hypernetted-chain (HNC) integral equation [25, 26] extended to the TCP (see, e.g., Refs. [16, 17]).

In the APEX model originally developed for the classical ionic OCP with bare Coulomb interaction to determine the effective field a second requirement is needed. In Ref. [9] the effective field $\mathcal{E}(r)$ is assumed as a Debye-Hückel-type screened interaction with unknown screening length. This free parameter is then adjusted in such a way to satisfy the exact second moment requirement. In contrast to the APEX the effective fields $\mathcal{E}_\alpha(r)$ in the PMFEX model are obtained automatically (see [16] for details) employing the thermodynamic perturbation theory [27]. We recall here these effective fields for completeness. For simplicity assuming Coulomb potential for the repulsive interactions, i.e. $\delta_{ee} = \delta_{ii} = 0$ (electron-electron and ion-ion interactions) and regularized one (see Eq. (4)) for electron-ion interactions these fields read [16]

$$\mathcal{E}_\alpha(r) = E_\alpha(r)\left\{1 + \frac{4\pi n_\alpha}{g_{\alpha R}(r)} \int_0^r \left[g_{\alpha\alpha}(\rho) - g_{ei}(\rho)\right] \rho^2 d\rho\right\}, \tag{27}$$

where $E_\alpha(r) = q_\alpha e_F / r^2$ are the bare single-particle fields. Based on the derivations given in Ref. [16] it is straightforward to show that the effective fields $\mathcal{E}_\alpha(r)$ can be alternatively represented as the logarithmic derivative of the radial distribution functions (RDF) $g_{\alpha R}(r)$ as

$$\mathcal{E}_\alpha(r) = \frac{k_B T}{Z_R e} \frac{\partial}{\partial r} \left[\ln g_{\alpha R}(r)\right] \tag{28}$$

which is known as the potential of mean force (PMF) approximation proposed by Yan and Ichimaru [13] (see also [25]). Using Eq. (12) we expand (26) around a value $\kappa = 0$ and find the second moment of the MFD in the PMFEX model

$$\left\langle E^2 \right\rangle_{\mathrm{PMFEX}} = \sum_\alpha 4\pi n_\alpha \int_0^\infty \mathcal{E}_\alpha(r)\, E_\alpha(r)\, g_{\alpha R}(r)\, r^2 dr. \tag{29}$$

Then, introducing Eq. (28) in Eq. (29) automatically satisfies the exact sum rule, $\langle E^2\rangle_{\mathrm{PMFEX}} = \langle E^2\rangle$, without any adjustable parameter. Here $\langle E^2\rangle$ is the exact second moment of the MFD derived in Ref. [16] for the TCP, see Eq. (A1). Thus, if the $g_{\alpha R}(r)$ are known the MFD within the PMFEX model and with the exact second moment can be calculated using Eqs. (9), (26), and (28).

The PMFEX effective field, Eq. (28), is valid for charged radiator with $Z_R \neq 0$. For a neutral radiator, i.e., in the limit $Z_R \to 0$, the PMF ansatz (28) is not applicable, as in this case the RDFs tend to unity, $g_{\alpha R} \to 1$, and $\ln g_{\alpha R}(r) \to 0$. Based on the derivations given in Refs. [16, 17] (see also Appendix A for details) the correct limit $Z_R \to 0$ can, however, be done and results in the effective field of Eq. (27), by setting $g_{\alpha R}(r) = 1$.

B. Renormalized cluster series

The comments at the end of Sec. III B and the success of PMFEX indicate that the Baranger-Mozer series could be improved if the single-particle fields in the functions $\chi_a^{(\alpha)}(\boldsymbol{\kappa})$ is replaced by a screened fields representing the effects of correlations in strongly coupled plasmas. In this spirit, a new functional series is obtained in terms of the renormalized functions $\psi_a^{(\alpha)}(\boldsymbol{\kappa})$ of Eq. (24) by the definition $\mathcal{L}^*[\psi_a;\boldsymbol{\kappa}] = \mathcal{L}[\chi_a;\boldsymbol{\kappa}]$ which is easily obtained from the BM series Eqs. (16)-(18) and the functional relationship between $\chi_a^{(\alpha)}$ and $\psi_a^{(\alpha)}$. Introducing the functions $\mathcal{R}_\alpha(r)$ by the relation $\mathcal{E}_\alpha(r) = \mathcal{R}_\alpha(r)\, E_\alpha(r)$ (we assume spherical symmetric interactions) with the effective $\mathcal{E}_\alpha(r)$ and single-particle $E_\alpha(r)$ fields, the functional relation between $\chi_a^{(\alpha)}$ and $\psi_a^{(\alpha)}$ is established as

$$\chi_a^{(\alpha)}(\boldsymbol{\kappa}) = \left[1 + \psi_a^{(\alpha)}(\boldsymbol{\kappa})\right]^{1/\mathcal{R}_\alpha(r_a)} - 1. \tag{30}$$

To obtain the new function $\mathcal{L}^*[\psi_a;\boldsymbol{\kappa}]$ which must be multi-linear with respect to ψ_a (cf. Eqs. (16)-(18)) we expand the $\chi_a^{(\alpha)}$-functions in Eq. (30) with respect to $\psi_a^{(\alpha)}$-functions [28]

$$\begin{aligned}\chi_a^{(\alpha)}(\boldsymbol{\kappa}) \;=\; & \frac{\psi_a^{(\alpha)}(\boldsymbol{\kappa})}{\mathcal{R}_\alpha(r_a)} + \frac{\left[\psi_a^{(\alpha)}(\boldsymbol{\kappa})\right]^2}{2!}\frac{1}{\mathcal{R}_\alpha(r_a)}\left[\frac{1}{\mathcal{R}_\alpha(r_a)} - 1\right] \\ & + \frac{\left[\psi_a^{(\alpha)}(\boldsymbol{\kappa})\right]^3}{3!}\frac{1}{\mathcal{R}_\alpha(r_a)}\left[\frac{1}{\mathcal{R}_\alpha(r_a)} - 1\right]\left[\frac{1}{\mathcal{R}_\alpha(r_a)} - 2\right] + ...\end{aligned} \tag{31}$$

Then elimination of $\chi_a^{(\alpha)}$ on the right side of equation $\mathcal{L}^*[\psi_a;\boldsymbol{\kappa}] = \mathcal{L}[\chi_a;\boldsymbol{\kappa}]$ using Eq. (31) yields the desired renormalized cluster series,

$$\mathcal{L}^*[\psi_a;\boldsymbol{\kappa}] = -\sum_\alpha \sum_{a=1}^\infty \frac{n_\alpha^a}{a!} H_a^{(\alpha)}(\boldsymbol{\kappa}) - \sum_{a=1}^\infty \frac{n_e^a}{a!} \sum_{b=1}^\infty \frac{n_i^b}{b!} H_{ab}^{(ei)}(\boldsymbol{\kappa}). \tag{32}$$

Here

$$H_a^{(\alpha)}(\boldsymbol{\kappa}) = \int \psi_1^{(\alpha)}(\boldsymbol{\kappa})\, \psi_2^{(\alpha)}(\boldsymbol{\kappa}) ... \psi_a^{(\alpha)}(\boldsymbol{\kappa})\, L_a^{(\alpha)}(\mathcal{T}_a^{(\alpha)}) d\mathcal{T}_a^{(\alpha)}, \tag{33}$$

$$\begin{aligned}H_{ab}^{(ei)}(\boldsymbol{\kappa}) \;=\; & \int \psi_1^{(e)}(\boldsymbol{\kappa})\, \psi_2^{(e)}(\boldsymbol{\kappa}) ... \psi_a^{(e)}(\boldsymbol{\kappa})\, \psi_1^{(i)}(\boldsymbol{\kappa})\, \psi_2^{(i)}(\boldsymbol{\kappa}) ... \psi_b^{(i)}(\boldsymbol{\kappa}) \\ & \times L_{ab}^{(ei)}(\mathcal{T}_a^{(e)}, \mathcal{T}_b^{(i)}) d\mathcal{T}_a^{(e)} d\mathcal{T}_b^{(i)}\end{aligned} \tag{34}$$

with the generalized Ursell functions $L_a^{(\alpha)}$ and $L_{ab}^{(ei)}$ which are recognized as the functional derivatives of $H_a^{(\alpha)}(\boldsymbol{\kappa})$ and $H_{ab}^{(ei)}(\boldsymbol{\kappa})$, respectively. Explicitly the first and second order generalized Ursell functions are found to be

$$L_1^{(\alpha)}(r_1) = \frac{g_{\alpha R}(r_1)}{\mathcal{R}_\alpha(r_1)}, \tag{35}$$

$$L_2^{(\alpha)}(\mathbf{r}_1,\mathbf{r}_2) = \frac{g_{\alpha\alpha}(|\mathbf{r}_1-\mathbf{r}_2|)-g_{\alpha R}(r_1)\,g_{\alpha R}(r_2)}{\mathcal{R}_\alpha(r_1)\,\mathcal{R}_\alpha(r_2)} - \frac{1}{n_\alpha}\delta(\mathbf{r}_1-\mathbf{r}_2)\,g_{\alpha R}(r_1)\,\frac{\mathcal{R}_\alpha(r_1)-1}{\mathcal{R}_\alpha^2(r_1)}, \tag{36}$$

$$L_{11}^{(ei)}(\mathbf{r}_1,\mathbf{R}_1) = \frac{g_{ei}(|\mathbf{r}_1-\mathbf{R}_1|)-g_{eR}(r_1)\,g_{iR}(R_1)}{\mathcal{R}_e(r_1)\,\mathcal{R}_i(R_1)} \tag{37}$$

which result the first three terms in Eq. (32)

$$\begin{aligned}\mathcal{L}^*(\boldsymbol{\kappa}) &= \mathcal{L}(\boldsymbol{\kappa}) = -\sum_\alpha n_\alpha \int \frac{\psi_1^{(\alpha)}(\boldsymbol{\kappa})}{\mathcal{R}_\alpha(r)} g_{\alpha R}(r)\,d\mathbf{r} \\ &-\sum_\alpha \frac{n_\alpha^2}{2}\left\{\int \frac{\psi_1^{(\alpha)}(\boldsymbol{\kappa})\,\psi_2^{(\alpha)}(\boldsymbol{\kappa})}{\mathcal{R}_\alpha(r_1)\,\mathcal{R}_\alpha(r_2)}\left[g_{\alpha\alpha}(|\mathbf{r}_1-\mathbf{r}_2|)-g_{\alpha R}(r_1)\,g_{\alpha R}(r_2)\right]d\mathbf{r}_1 d\mathbf{r}_2\right. \\ &\left.+\frac{1}{n_\alpha}\int\left[\psi_1^{(\alpha)}(\boldsymbol{\kappa})\right]^2\frac{1-\mathcal{R}_\alpha(r_1)}{\mathcal{R}_\alpha^2(r_1)}g_{\alpha R}(r_1)\,d\mathbf{r}_1\right\} \\ &-n_e n_i\int\frac{\psi_1^{(e)}(\boldsymbol{\kappa})\,\psi_1^{(i)}(\boldsymbol{\kappa})}{\mathcal{R}_e(r_1)\,\mathcal{R}_i(R_1)}\left[g_{ei}(|\mathbf{r}_1-\mathbf{R}_1|)-g_{eR}(r_1)\,g_{iR}(R_1)\right]d\mathbf{r}_1 d\mathbf{R}_1.\end{aligned} \tag{38}$$

The first term of Eq. (38) is seen to be precisely PMFEX (cf. Eq. (23) and (25)). The factor $\mathcal{R}_\alpha(r)$ occurs automatically here from the renormalization and eliminates the assumption (25) of PMFEX.

Finally the angular integration in Eq. (38) can be performed using spherical harmonic expansion [28]. This yields

$$\mathcal{L}(\kappa) = \mathcal{L}_{\mathrm{PMFEX}}(\kappa) + \Delta\mathcal{L}(\kappa), \tag{39}$$

where the first term is the PMFEX result, Eq. (26), and the second term represents the corrections due to the renormalization,

$$\begin{aligned}\Delta\mathcal{L}(\kappa) &= 2\pi\sum_\alpha n_\alpha\int_0^\infty\left[j_0(2\kappa\mathcal{E}_\alpha(r))-2j_0(\kappa\mathcal{E}_\alpha(r))+1\right]\frac{\mathcal{R}_\alpha(r)-1}{\mathcal{R}_\alpha^2(r)}g_{\alpha R}(r)\,r^2dr \\ &-4\sum_\alpha n_\alpha\int_0^\infty G_{\alpha\alpha}(\kappa,k)\left[S_{\alpha\alpha}(k)-1\right]k^2dk - 8\frac{n_e n_i}{n}\int_0^\infty G_{ei}(\kappa,k)\,S_{ei}(k)\,k^2dk \\ &+\frac{1}{2}\left[\mathcal{L}_{\mathrm{PMFEX}}^2(\kappa)-\mathcal{L}_0^2(\kappa)\right].\end{aligned} \tag{40}$$

Here $\mathcal{L}_0(\kappa)$ is the $\mathcal{L}_{\mathrm{PMFEX}}(\kappa)$ given by Eq. (26) but with $g_{\alpha R}(r)=1$,

$$\mathcal{L}_0(\kappa) = \sum_\alpha 4\pi n_\alpha\int_0^\infty\frac{1-j_0(\kappa\mathcal{E}_\alpha(r))}{\mathcal{R}_\alpha(r)}r^2dr. \tag{41}$$

In Eq. (40) the term $S_{\alpha\beta}(k)$ (with $\alpha,\beta=e,i$) is the static structure factor for the two-component plasma,

$$S_{\alpha\beta}(k) = \delta_{\alpha\beta} + 4\pi n_{\alpha\beta}\int_0^\infty\left[g_{\alpha\beta}(r)-1\right]j_0(kr)\,r^2dr \tag{42}$$

with $\delta_{\alpha\alpha}=1$, $\delta_{ei}=0$, $n_{\alpha\alpha}=n_\alpha$, $n_{ei}=n=n_e+n_i$, and $G_{\alpha\beta}(\kappa,k)$ is defined by

$$G_{\alpha\beta}(\kappa,k) = \sum_{l=0}^\infty(-1)^l(2l+1)\,J_l^{(\alpha)}(\kappa,k)\,J_l^{(\beta)}(\kappa,k), \tag{43}$$

$$J_l^{(\alpha)}(\kappa,k) = \int_0^\infty j_l(kr)\left[j_l(\kappa\mathcal{E}_\alpha(r))-\delta_{l0}\right]\frac{r^2dr}{\mathcal{R}_\alpha(r)}. \tag{44}$$

TABLE I: The critical values $\sigma_c(Z,\delta)$ for some values of the ion charge Z and three values of $\delta = 0.1a$, $0.2a$ and $0.4a$.

δ	H^+	Li^{3+}	B^{5+}	N^{7+}	Al^{13+}	Ca^{20+}
$0.1a$	6.87	7.59	7.67	7.62	7.59	7.63
$0.2a$	6.55	7.68	7.52	7.13	6.66	6.48
$0.4a$	8.90	12.73	10.76	9.39	6.75	6.00

Also, $j_l(x)$ is the spherical Bessel function of order l. It should be noted that for deriving the renormalized series Eq. (32) we do not use explicit functional form of $\mathcal{E}_\alpha(r)$. Hence, in spite of its important role in the theory, the precise functional form of the effective field $\mathcal{E}_\alpha(r)$ may remain arbitrary. Moreover, it is straightforward to show that the generating function Eq. (16) as well as its renormalized version Eq. (32) yield the exact even moments of the MFD according to Eq. (12) independently of the functional form of $\mathcal{E}_\alpha(r)$. In the present context it might appear more reasonable to choose $\mathcal{E}_\alpha(r)$ to improve convergence of the renormalized series Eq. (32). A similar procedure is used in thermodynamic perturbation theory where the corresponding parameters of the leading term are chosen to make the next order terms vanish [29]. But this is not possible without making $\mathcal{E}_\alpha(r)$ a function of $\boldsymbol{\kappa}$ (see similar discussion in Ref. [11] in the context of APEX). Here we consider for $\mathcal{E}_\alpha(r)$ the mean-force field as derived in Ref. [16] for the TCP (see also Eq. (28) as well as Eq. (27) for the repulsive Coulomb interactions) and which appears automatically from the second moment condition $\partial^2\mathcal{L}^*/\partial\kappa^2\big|_{\kappa=0} = \frac{1}{3}\langle E^2\rangle$ for the renormalized function $\mathcal{L}^*$ (32). The theoretical scheme resulting from Eqs. (39)-(44) is abbreviated as PMFEX+. It agrees for neutral points quite well with the molecular dynamic (MD) simulation results, as we will show in the next section. It is straightforward to show that the correction $\Delta\mathcal{L}(\kappa)$ in Eq. (39) behaves as $\sim \kappa^4$ at $\kappa \to 0$ and, therefore, does not contribute to the second moment. Then the quantity $\langle E^2\rangle$ receives contribution only from the PMFEX term in Eq. (39).

V. APPLICATION TO THE NEUTRAL RADIATOR

In the case of neutral radiator, $Z_R = 0$, the plasma-radiator correlation function is $g_{\alpha R}(r) = 1$ and Eq. (40) is simplified. In particular, the last term vanishes since $\mathcal{L}_{\mathrm{PMFEX}}(\kappa) = \mathcal{L}_0(\kappa)$ for $g_{\alpha R}(r) = 1$. Thus, the generating function $\mathcal{L}(\kappa)$ of the MFD in the PMFEX+ model is given by $\mathcal{L}(\kappa) = \mathcal{L}_0(\kappa) + \Delta\mathcal{L}(\kappa)$, where $\mathcal{L}_0(\kappa)$ is the ordinary PMFEX expression, with $g_{\alpha R}(r) = 1$, see Eq. (41). The higher order corrections are involved in the second term, $\Delta\mathcal{L}(\kappa)$. The functions $\mathcal{R}_\alpha(r)$ are obtained from Eq. (27),

$$\mathcal{R}_\alpha(r) = 1 + 4\pi n_\alpha \int_0^r \left[g_{\alpha\alpha}(\rho) - g_{ei}(\rho)\right]\rho^2 d\rho \tag{45}$$

which in the limit of small plasma-parameters ($\Gamma_{ee} \to 0$) can be evaluated explicitly using the Debye-Hückel approximation, $\mathcal{R}_e(r) = \mathcal{R}_i(r) \simeq \left(\frac{r}{\lambda}+1\right)e^{-r/\lambda}$. Here $\lambda^2 = \varepsilon_0 k_B T/(Zne^2)$ is the Debye screening length. Thus similar to the standard PMFEX, the PMFEX+ approximation links the MFD to the RDFs. To obtain explicit results for the MFD the corresponding RDFs and the static structure factors must be determined first. This is done by solving numerically the hypernetted chain (HNC) integral equations [25, 26] for the TCPs under consideration (see Ref. [16] and references therein for more details). For simplicity we here assume bare Coulomb interaction for electron-electron and ion-ion, i.e. $\delta_{ee} \simeq 0$ and $\delta_{ii} \simeq 0$, and a regularized ion-electron interaction with a parameter $\delta_{ei} = \delta$ fixed to $\delta = 0.2a$ or $\delta = 0.4a$, where $a = (4\pi n/3)^{-1/3}$ is the Wigner-Seitz radius. For this kind of TCPs, the HNC method has already been extensively tested and evaluated by comparison of the resulting RDFs with those obtained by classical MD simulations [16]. For the numerical solution of the HNC scheme the dimensionless parameter $\sigma_{ei} = Ze_S^2 u_{ei}(0)/k_B T = \Gamma_{ei}(a/\delta)$, i.e. the maximum value of the electron-ion interaction energy in units of $k_B T$, plays an important role (see also [15, 16]). Within our numerical treatment of the HNC equations a parameter regime with $\sigma_{ei} < \sigma_c(Z,\delta)$ is accessible, where the critical values σ_c for $\delta = 0.1a$, $0.2a$ and $0.4a$ and the different studied TCPs (H^+, Li^{3+}, B^{5+}, N^{7+}, Al^{13+} and Ca^{20+}) are given in Table I. Beyond this value the HNC numerical procedure does either not converge or ends up in unphysical solutions. A similar behavior has been reported in Ref. [15] for the case of an ion embedded in electrons. With the RDFs and $S_{\alpha\beta}(k)$ provided by the HNC scheme the MFD $P(E)$ in the PMFEX+ model is then calculated via Eqs. (9) and (39)-(45) by standard numerical differentiation and integration methods [30]. In practice it appears sufficient to terminate the sum in Eq. (43) at $l = 5$.

To test the PMFEX+ approximation and improvements compared to the standard PMFEX approach the calculated MFDs are confronted with those obtained by classical MD simulations. In the MD simulations the classical equations

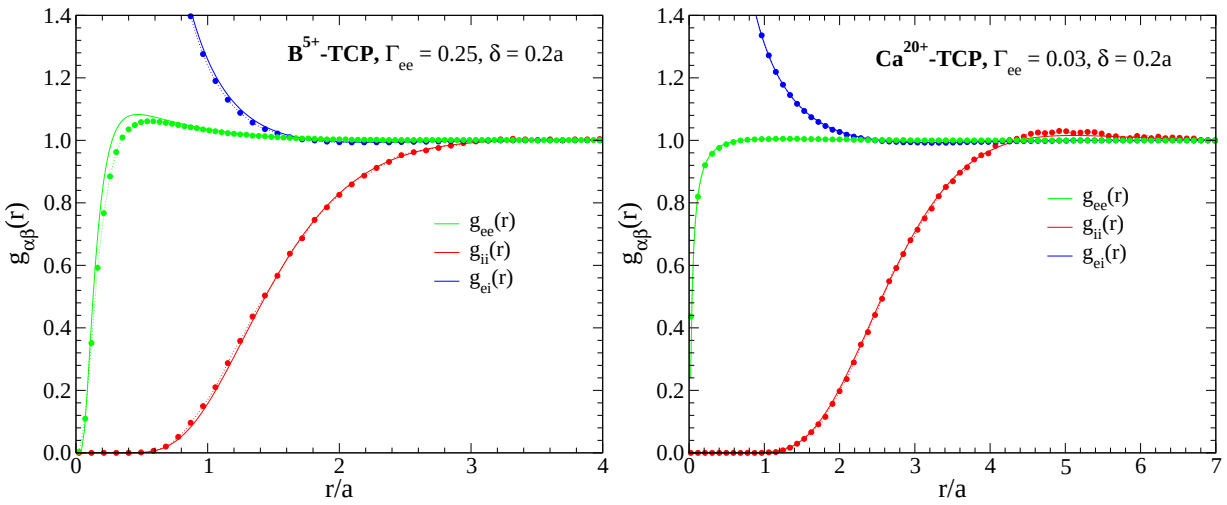

FIG. 1: RDFs $g_{\alpha\beta}(r)$ for B^{5+} (left panel) and Ca^{20+} (right panel) plasmas with $\delta = 0.2a$, $\Gamma_{ee} = 0.25$ and $\Gamma_{ee} = 0.03$, respectively. The lines correspond to the HNC approximation while the symbols denote the MD simulations. The different lines represent g_{ee} (green), g_{ii} (red) and g_{ei} (blue).

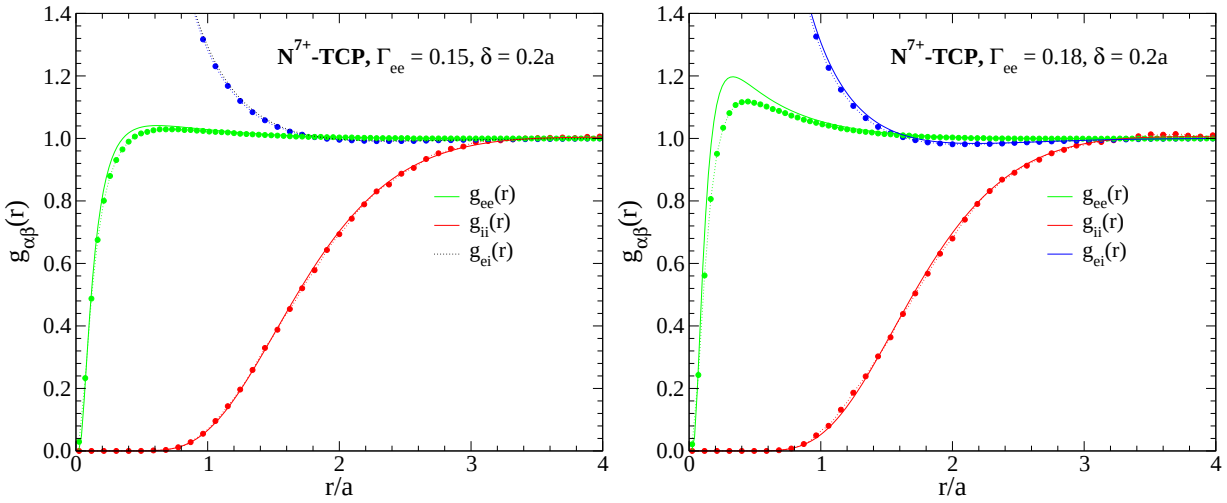

FIG. 2: Same as Fig. 1 for N^{7+} plasma with $\delta = 0.2a$, $\Gamma_{ee} = 0.15$ (left panel) and $\Gamma_{ee} = 0.18$ (right panel).

of motion are numerically integrated for N_i ions and $N_e = ZN_i$ electrons interacting via the regularized potentials $u_{\alpha\beta}(r)$. Such MD simulations have already been extensively tested and successfully applied for investigations of the dynamic properties [31, 32, 33, 34, 35, 36] and the MFDs [16, 17] of a TCP with regularized potentials (see also Ref. [38] and references therein). For our present considerations we investigated the specific cases of H^+, Li^{3+}, B^{5+}, N^{7+}, Al^{13+} and Ca^{20+} TCPs with symmetric (hydrogen) and strongly asymmetric densities of the plasma species and certain values of the coupling parameters $\Gamma_{\alpha\beta}$ with $\alpha, \beta = e, i$. These coupling parameters $\Gamma_{\alpha\beta}$, at a given parameter δ, are chosen to avoid the mentioned numerical difficulties with the HNC scheme and the formation of unphysical bound states in the classical MD simulations. This implies in particular that for highly charged plasma ions with $Z \gg 1$ plasma states with strongly correlated ions ($\Gamma_{ii} \gg 1$) and strong electron-ion interactions ($\Gamma_{ei} \sim 1$) are accessible, while the parameter Γ_{ee} has to remain quite small, $\Gamma_{ee} \simeq \Gamma_{ei}/Z \ll 1$. But in the case of highly charged ions even for $\Gamma_{ee} \ll 1$ the electrons may be strongly correlated due to nonlinear effects as will be discussed below. The MD simulations providing the present MFDs and RDFs have been performed using $N_{\rm MD} = N_i + N_e = 5376$ particles. Further details on the applied MD technique can be found in Refs. [31, 32, 33, 34]. As the theoretical models and the numerical solutions depend directly on the coupling parameters $\Gamma_{\alpha\beta}$ and the regularization parameter δ we discuss, as e.g. in Refs. [15, 16, 17], our results in terms of these parameters rather than in the underlying physical values of density and temperature.

Before discussing the MFD itself, we first consider briefly the RDFs and the validity of the HNC approximation

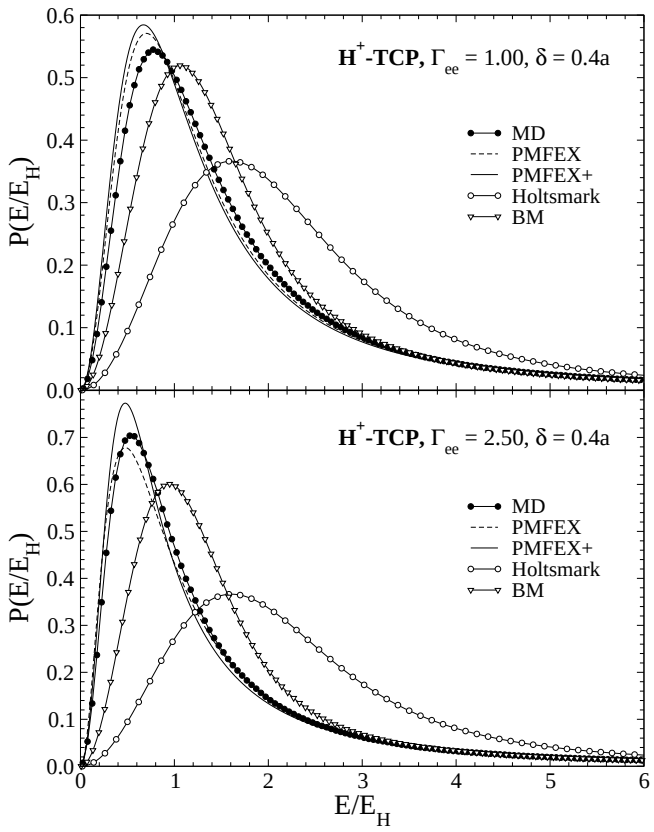

FIG. 3: Normalized electric microfield distributions for a hydrogen plasma with $\delta = 0.4a$, $\Gamma_{ee} = \Gamma_{ii} = 1$, $\sigma_{ei} = 3.15$ (top) and $\Gamma_{ee} = \Gamma_{ii} = 2.5$, $\sigma_{ei} = 7.87$ (bottom) as a function of the electric field in units of E_H. The dashed and the solid curves are the results of the PMFEX and PMFEX+, respectively. The filled circles represent the MFD from the MD simulations. The Holtsmark and standard Baranger-Mozer distributions are also shown as open circles and triangles, respectively.

for the parameters at hand. For small and moderate coupling where the parameter σ_{ei} is well below the critical value σ_c, the RDFs as either calculated by the HNC scheme or extracted from the MD simulations are always in perfect agreement (see e.g. the corresponding examples given in [16]). Some typical examples for the RFDs at rather large coupling, where some deviations between HNC and MD may show up, are given in Figs. 1 and 2. Due to the regularization of the ion-electron interaction the RDF $g_{ei}(r)$ is finite in the limit $r \to 0$ (not visible in Figs. 1 and 2) and can be approximated as $g_{ei}(0) \simeq \exp(\sigma_{ei}/\mathcal{R})$ with $\mathcal{R} = 1 + (\delta/a)(3\Gamma_{ei})^{1/2}$, see Refs. [15, 16]. Thus the RDF $g_{ei}(r)$ shows the expected growth of correlations with increased coupling and decreased regularization parameter, where the HNC scheme tends to overestimate the value of $g_{ei}(0)$ (not visible in the figures). For example, for N^{7+} ions $g_{ei}^{\rm HNC}(0) \simeq 57.4$, $g_{ei}^{\rm MD}(0) \simeq 48.8$ and $g_{ei}^{\rm HNC}(0) \simeq 107.3$, $g_{ei}^{\rm MD}(0) \simeq 96.4$ with $\delta = 0.2a$, $\Gamma_{ee} = 0.15$ and $\Gamma_{ee} = 0.18$, respectively. At strong coupling deviations also occur in the electron-electron RDF $g_{ee}(r)$ at small r (as in the case of B^{5+} and N^{7+}). The strong electron-ion interaction increases the electron density around the highly charged ion which introduces additional correlations between the electrons. This increases the probability of close electronic distances and results in the maxima in $g_{ee}(r)$ at distances $r \lesssim a$. This effect is obviously again overestimated in the HNC approach.

In Figs. 3-8 we next compare the MFDs calculated from the PMFEX (dashed lines) and PMFEX+ (solid lines) schemes as well as from MD simulations (filled circles) where the electric microfields are scaled in units of the Holtsmark field E_H [see Eq. (3)]. The open circles are the Holtsmark MFDs for a TCP with Coulomb potential and the MFDs predicted by the first two terms of the standard BM series Eqs. (15)-(21) are also shown as triangles. We here focus on cases of strong coupling where the PMFEX and PMFEX+ results significantly differ, i.e. where the higher order corrections $\Delta\mathcal{L}(\kappa)$ (41) substantially contribute to the generating function $\mathcal{L}(\kappa) = \mathcal{L}_0(\kappa) + \Delta\mathcal{L}(\kappa)$. As can be seen in all the presented cases the MFDs obtained both from the PMFEX and the PMFEX+ treatment strongly differ from the standard BM electric field distributions.

Concerning the agreement with the MD simulations the PMFEX+ scheme turns out to improve the PMFEX model substantially for large charge states of the plasma ions. For H^+, Fig. 3, no improvement can be found, and the agreement with the MD simulations remains rather unsatisfactory, although the PMFEX(+) methods yield a much

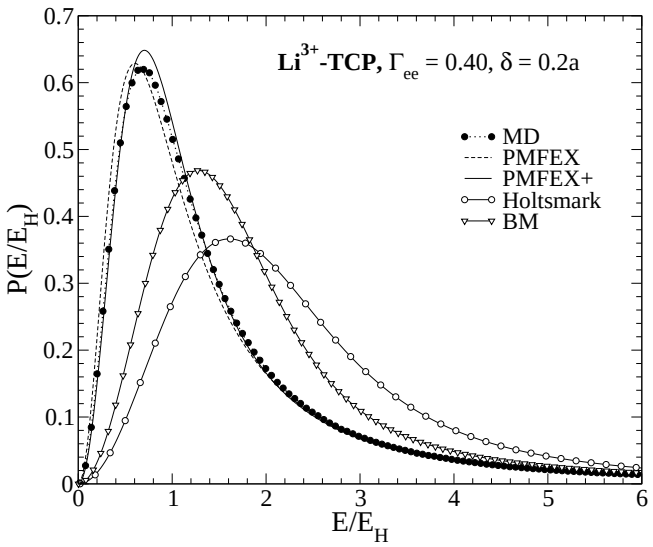

FIG. 4: Same as Fig. 3 for Li^{3+} plasma with $\Gamma_{ee} = 0.4$, $\Gamma_{ii} = 2.5$, $\sigma_{ei} = 6.6$ and $\delta = 0.2a$.

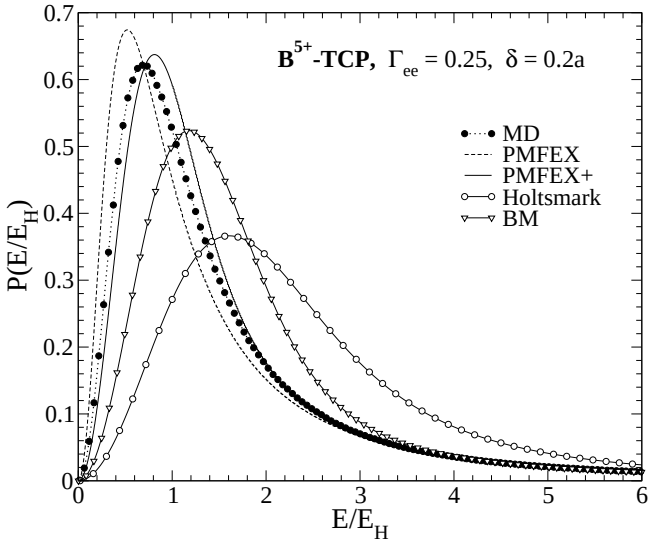

FIG. 5: Same as Fig. 3 for B^{5+} plasma with $\Gamma_{ee} = 0.25$, $\Gamma_{ii} = 3.66$, $\sigma_{ei} = 6.64$ and $\delta = 0.2a$.

better description of the MFD than the standard BM approach. For Li^{3+} and B^{5+}, Figs. 4 and 5, the PMFEX+ scheme much better agrees with the MD than the PMFEX, but obviously still deserves further improvement. However, for ion charges $Z > 5$, Figs. 6-8, the MFDs obtained from MD simulations are in excellent agreement with those predicted by PMFEX+ (except for some smaller values near the maxima). The rather large deviation of PMFEX from PMFEX+ towards a higher probability of low fiels (in particular in Figs. 6 and 8) indicates that the PMFEX applied to the field at a neutral point does not correctly account for perturber-perturber correlations, and, therefore, underestimates the MFDs at large fields. As expected for $Z_R = 0$ all distributions shown in Figs. 3-8 merge at large electric fields, $\eta = E/E_H \gtrsim 6$ with the Holtsmark distribution with the asymptotic behavior $P_H(\eta) \simeq 1.496\eta^{-2.5}$. This indicates that due to electron-electron and ion-ion Coulomb interactions with $\delta_{ee} \simeq \delta_{ii} \simeq 0$ the second moments of the MFDs shown in Figs. 3-8 do not exist, see e.g. Eq. (A7) derived in Appendix A.

To gain some more insight of the features and the range of validity of the PMFEX and PMFEX+ models we consider the extreme regimes of Figs. 9 and 10 with further increased coupling parameters. In the PMFEX scheme and for large values of Γ_{ee} the effective fields at large distances behave as $\mathcal{E}_\alpha(r) \sim \frac{1}{r}e^{-ar}\cos(br)$. Here a and b are some parameters increasing with Γ_{ee}, whereby the involved screening length a^{-1} does not necessarily coincide with the Debye length λ. The oscillatory nature of the effective fields drastically changes the properties of the generating function $\mathcal{L}_0(\kappa)$ in the PMFEX approximation (see Eq. (41)), which becomes negative at $\kappa E_H \gtrsim 1$. This is not the

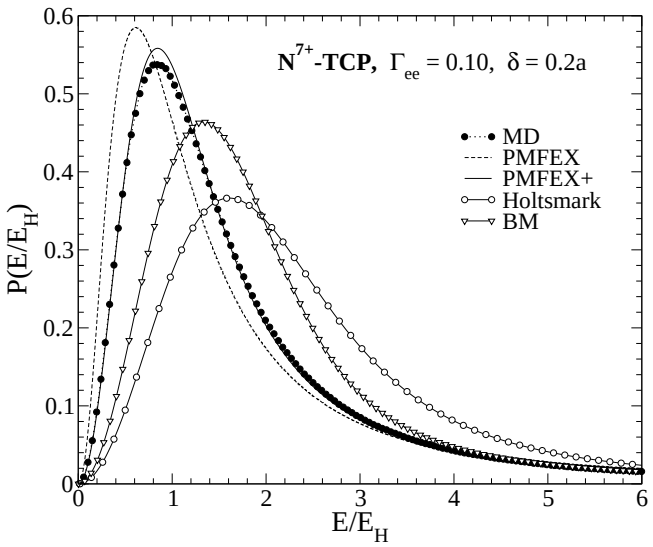

FIG. 6: Same as Fig. 3 for N^{7+} plasma with $\Gamma_{ee} = 0.1$, $\Gamma_{ii} = 2.56$, $\sigma_{ei} = 3.66$ and $\delta = 0.2a$.

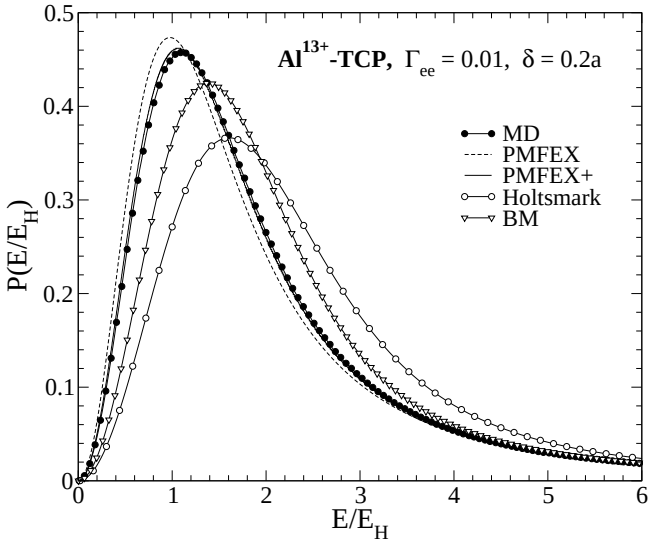

FIG. 7: Same as Fig. 3 for Al^{13+} plasma with $\Gamma_{ee} = 0.01$, $\Gamma_{ii} = 0.72$, $\sigma_{ei} = 0.67$ and $\delta = 0.2a$.

case in APEX (as well as in PMFEX for charged impurity ion, i.e. for the MFD at charged point) where the effective field is treated in the Debye-Hückel form and thus is positive and decreases monotonically with r. Therefore the κ-integration in Eq. (9) diverges and hence the PMFEX model becomes invalid for neutral radiators ($Z_R = 0$) (and no curves for the PMFEX can be given in Figs. 9 and 10). But even in this extreme regime the PMFEX+ model remains valid and the agreement with MD simulations is still quite good for the lower charge state $Z = 7$ shown in Fig. 9 (although not as good as in Fig. 6), and almost perfect for the highly charged ions as shown in Fig. 10.

As discussed above some deviations between HNC scheme and MD simulations occur in the electron-electron RDF $g_{ee}(r)$ at small distances $r \lesssim a$ for B^{5+} and N^{7+} TCPs, see the left panel of Fig. 1 and Fig. 2. Similarly the static structure factor $S_{ee}(k)$ obtained from HNC deviates from MD data at $ka \gtrsim 1$. This may be critical for the accuracy of the electronic effective field, Eq. (45) and hence for the generating function $\mathcal{L}(\kappa)$ Eqs. (39)-(41) calculated from the HNC approximation. Since the generating function is involved in the exponential factor $e^{-\mathcal{L}(\kappa)}$ even small deviations in $\mathcal{L}(\kappa)$ results some appreciable deviations in the MFD. Apparently the PMFEX+ model could be improved in the case of B^{5+} and N^{7+} TCPs in Figs. 5 and 9, respectively, using the MD data for the RDF $g_{ee}(r)$.

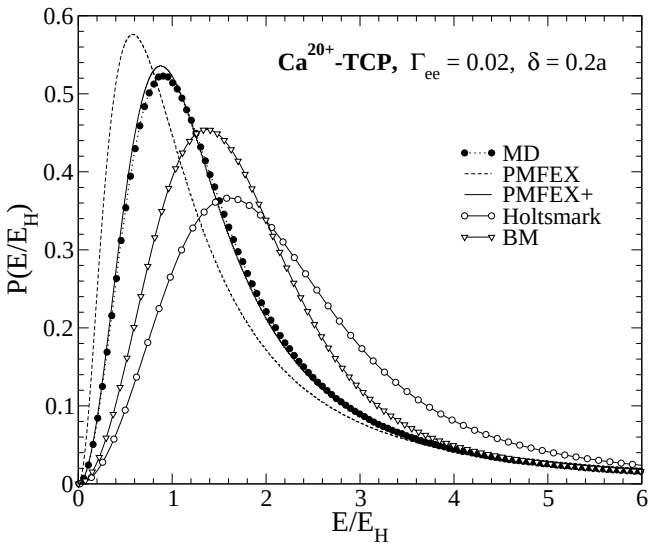

FIG. 8: Same as Fig. 3 for Ca^{20+} plasma with $\Gamma_{ee} = 0.02$, $\Gamma_{ii} = 2.95$, $\sigma_{ei} = 2.03$ and $\delta = 0.2a$.

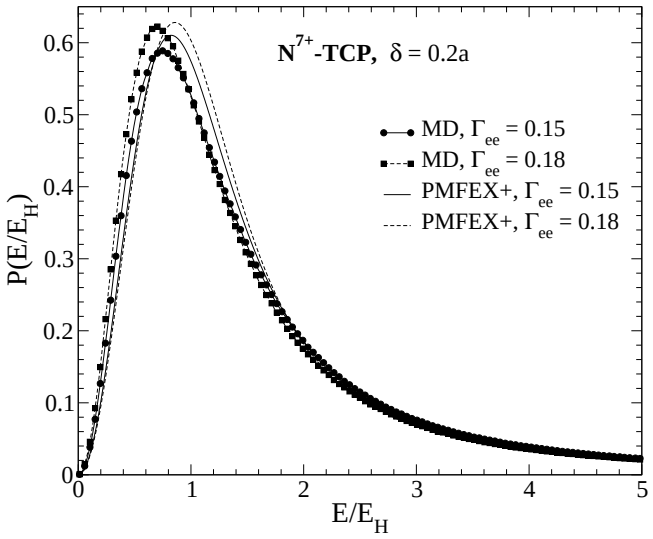

FIG. 9: Normalized electric microfield distributions for N^{7+} plasma with $\Gamma_{ee} = 0.15$ ($\Gamma_{ii} = 3.85$, $\sigma_{ei} = 5.49$), $\Gamma_{ee} = 0.18$ ($\Gamma_{ii} = 4.61$, $\sigma_{ei} = 6.59$), and $\delta = 0.2a$ as a function of the electric field in units of E_H. The solid and dashed curves are the results of the PMFEX+ model. The filled circles and squares represent the MFDs from the MD simulations.

VI. DISCUSSION AND CONCLUSION

In this paper we investigate the microfield distributions in a two-component plasmas with attractive electron-ion interactions. Based on the renormalization of the standard Baranger-Mozer cluster expansion technique our objective here was to derive the corrections to the PMFEX model proposed recently in Ref. [16]. The outlined theoretical method is abbreviated as PMFEX+. In general the MFDs predicted by PMFEX for the case of charged impurity ion are very accurate and its corrections may be quite small, except the case of strongly coupled hydrogen at small regularization parameter δ [16]. As discussed in Ref. [17] the PMFEX is less accurate in the case of the neutral point and an improvement of the model is required. We thus focused on testing the predictions of the PMFEX+ approximation for the neutral point based on the HNC treatment of static correlations by confronting it with the MFDs obtained from MD simulations. One of the basic assumptions made for all these models is the regularization of the attractive electron-ion interaction at short distances to introduce quantum diffraction effects in the employed classical approach. For the repulsive electron-electron and ion-ion interactions we assumed a bare Coulomb potential, for simplicity.

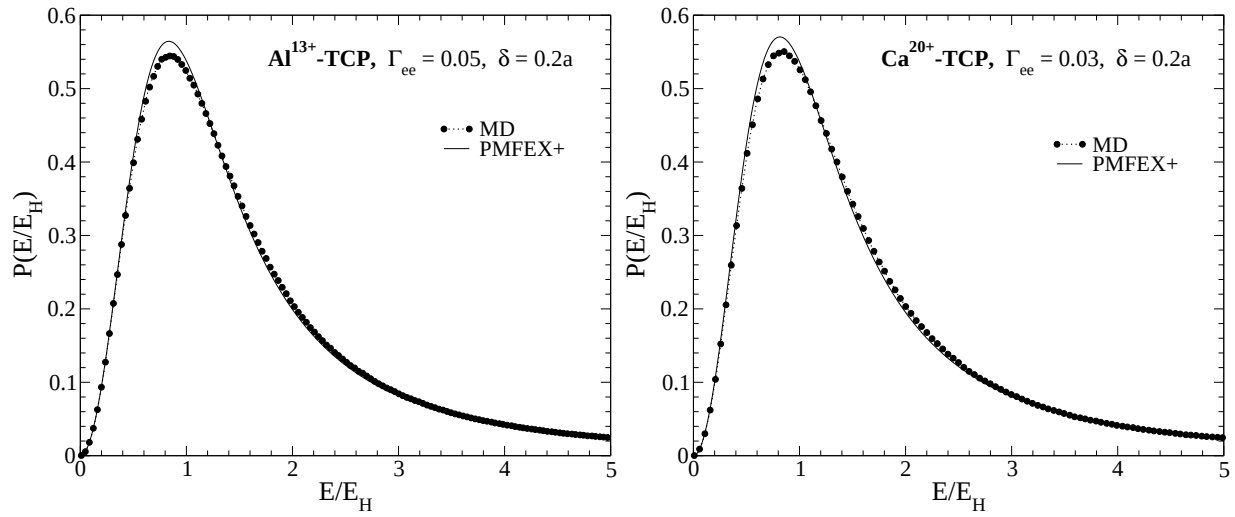

FIG. 10: Same as Fig. 9 for Al^{13+} (left panel) and Ca^{20+} (right panel) plasmas with $\delta = 0.2a$, $\Gamma_{ee} = 0.05$, $\Gamma_{ii} = 3.59$, $\sigma_{ei} = 3.33$ and $\Gamma_{ee} = 0.03$, $\Gamma_{ii} = 4.42$, $\sigma_{ei} = 3.05$, respectively.

As examples the cases of H^+, Li^{3+}, B^{5+}, N^{7+}, Al^{13+} and Ca^{20+} two-component plasmas (TCPs) with symmetric and largely asymmetric densities of the plasma species were considered. Our treatment is limited to a parameter regime with $\sigma < \sigma_c$, where the critical values σ_c for $\delta = 0.1a$, $0.2a$ and $0.4a$ are shown in Table I. Within this parameter regime the $g_{\alpha\beta}(r)$ from the HNC equations agree well with the MD simulations (except the correlation function $g_{ee}(r)$ for the cases given in Figs. 1 and 2). Beyond these critical σ the HNC equations do either not converge or end up in unphysical solutions. A further increase of the coupling parameters also leads to the formation of classical bound electronic states in the MD simulations with no corresponding quantum counterpart.

For high ion charges $Z > 5$, like N^{7+}, Al^{13+} and Ca^{20+} the PMFEX model is substantially improved and the agreement of the PMFEX+ model with the MD simulations is excellent, as shown in Figs. 6-8 and 10. For a TCP with light ions, e.g. the case of Li^{3+} ions in Fig. 4, the PMFEX and PMFEX+ differ, but both somewhat deviate from the MD simulations as in the case of H^+ TCP. In this regime with moderate ionic charge state Z and for large coupling the renormalized Baranger-Mozer series should probably be truncated at higher orders. We have also shown that with increasing coupling the PMFEX scheme becomes invalid while the PMFEX+ approach still works and yields good or even almost perfect agreement with the MD, see Figs. 9 and 10.

In summary we note that the PMFEX approximation incorporates some key features of the MFD, in particular for large microfields E (small κ values). The large fields are predominantly due to configurations with a single-plasma particle near the impurity ion. In this case the perturber-perturber correlations are less important and the PMFEX as an independent-particle model is accurate for both neutral and charged radiators. The behavior of the MFD at large E is closely related to the behavior of the generating function $\mathcal{L}(\kappa)$ at small κ and how much accurate the exact second moment is involved in the model. At small κ the generating function behaves as $\mathcal{L}(\kappa) \simeq (\kappa^2/6)\langle E^2\rangle$ (see Eq. (12)), where the second moment $\langle E^2\rangle$ is exactly involved in the PMFEX model. Furthermore the microfields in the large field regime are asymptotically Gaussian distributed and characterized by the second moment $\langle E^2\rangle$. As discussed above this is, however, not so for a neutral radiator and assuming bare Coulomb interactions between plasma particles where $\mathcal{L}(\kappa)$ behaves as $\sim \kappa^{3/2}$ at small κ and the MFDs is similar to the Holtsmark distribution at large E. Conversely, the small microfields (large κ values) are due to the additive effects of many particles at large distances and the PMFEX approximation is again accurate [16] except in the case of the neutral point where some deviations from MD simulations may occur, see Figs. 3-8 and Ref. [17] for other examples. The main uncertainty in PMFEX, therefore, remains the domain of the intermediate configurations with $E \sim 1$ and $\kappa \sim 1$ (in units of E_H and $1/E_H$, respectively). Apparently, this domain is reduced by means of the renormalized (screened) fields $\mathcal{E}_\alpha(r)$ and the PMFEX is much more adequate compared to the standard Baranger-Mozer (second order) treatment. In PMFEX+ model, on the other hand, imposing the renormalization procedure to the standard Baranger-Mozer series substantially improves their convergency, since $\psi_a^{(\alpha)}(\boldsymbol{\kappa})$ tends to zero for the relevant configurations more rapidly than $\chi_a^{(\alpha)}(\boldsymbol{\kappa})$. Finally, the PMFEX+ model may also be useful for a charged impurity ion in the cases where the PMFEX approximation deviates from MD. For the TCP, an example is the case of strongly coupled hydrogen with small regularization parameter δ considered in Ref. [16].

Acknowledgments

This work was supported by the Bundesministerium für Bildung und Forschung (BMBF, 06ER145) and by the Gesellschaft für Schwerionenforschung (GSI, ER/TOE). The work of H.B.N. and D.A.O. has been partially supported by the Armenian Ministry of Higher Education and Science Grant No. 0247. We gratefully acknowledge many stimulating discussions with C. Toepffer.

APPENDIX A: EXACT SECOND MOMENT FOR NEUTRAL RADIATOR

In this Appendix we derive the exact second moment for the MFD in the TCP at the neutral point. We use the exact relation for the second moment derived in Ref. [16]

$$\left\langle E^2\right\rangle = \frac{k_B T n_e}{Z_R \varepsilon_0}\left(\int_0^\infty \widetilde{u}_e\left(r\right) g_{eR}\left(r\right) dr - \int_0^\infty \widetilde{u}_i\left(r\right) g_{iR}\left(r\right) dr\right), \tag{A1}$$

where $\widetilde{u}_\alpha\left(r\right) = -\left[r^2 u'_{\alpha R}\left(r\right)\right]'$ with $\alpha = e, i$ and the pair interaction potentials $u_{\alpha R}\left(r\right)$ are given by Eq. (4) with the regularization parameters $\delta_{\alpha R}$.

The second moment $\left\langle E^2\right\rangle$ is ill-defined for the neutral-point distribution since $Z_R \to 0$ and $g_{\alpha R}\left(r\right) \to 1$ and the expression in the brackets in Eq. (A1) vanishes in this case (this is true for the Coulomb potential as well as for any potential regularized at the origin). To obtain the correct limit of Eq. (A1) at $Z_R \to 0$ we recall the definition of the correlation functions $g_{\alpha R}\left(r\right)$ [16]. At vanishing Z_R this functions read

$$g_{\alpha R}(r) - 1 = -\frac{Z_R e_S^2}{k_B T}\left\{q_\alpha u_{\alpha R}\left(r\right) + \sum_\beta q_\beta n_\beta \int d\mathbf{r}_1 u_{\beta R}\left(r_1\right)\left[g_{\alpha\beta}\left(\left|\mathbf{r} - \mathbf{r}_1\right|\right) - 1\right]\right\} + \mathrm{O}\left(Z_R^2\right). \tag{A2}$$

Here $g_{\alpha\beta}\left(r\right)$ are the equilibrium correlation functions. Note that the second term in the right-hand side of Eq. (A2) is the excess potential energy of the TCP. In particular, using Eq. (A2) it is straightforward to calculate the effective field $\mathcal{E}_\alpha\left(r\right)$ for the neutral point. Insertion of this relation into Eq. (28) in the limit $Z_R \to 0$ and for Coulomb electron-electron, ion-ion interactions yield Eq. (27) with $g_{\alpha R}\left(r\right) = 1$ (see also Eq. (45)).

Now we substitute Eq. (A2) into Eq. (A1). In the limit of vanishing charge $Z_R \to 0$ this yields

$$\begin{aligned}\left\langle E^2\right\rangle &= 4\pi\sum_\alpha n_\alpha \int_0^\infty E_\alpha^2\left(r\right) r^2 dr \\ &+16\pi^2 n_e^2 e_F^2\left\{\sum_\alpha \int_0^\infty \left[g_{\alpha\alpha}\left(r\right) - 1\right]\Psi_{\alpha\alpha}\left(r\right) r dr - 2\int_0^\infty \left[g_{ei}\left(r\right) - 1\right]\Psi_{ei}\left(r\right) r dr\right\},\end{aligned} \tag{A3}$$

where $E_\alpha\left(r\right) = -q_\alpha e_F u'_{\alpha R}\left(r\right)$ is the single-particle electric field with $q_e = -1$ and $q_i = Z$, $U_\beta\left(r\right) = \left[r u_{\beta R}\left(r\right)\right]'$, and

$$\Psi_{\alpha\beta}\left(r\right) = \frac{1}{2}\int_0^\infty \left[U_\beta\left(\left|\rho - r\right|\right) - U_\beta\left(\rho + r\right)\right] u_{\alpha R}\left(\rho\right)\rho d\rho. \tag{A4}$$

The first term in Eq. (A3) is the averaged density of the electric microfield energy (self-energy), the second one is the density of the excess electric energy which appears due to the correlations between plasma particles. Assuming regularized interaction potential Eq. (4) we obtain $U_\beta\left(r\right) = e^{-r/\delta_{\beta R}}/\delta_{\beta R}$, and

$$\Psi_{ei}\left(r\right) = 1 - \frac{1}{2}e^{-r/\delta_{iR}} - \frac{e^{-r/\delta_{eR}} - e^{-r/\delta_{iR}}}{2\left(1-\Delta\right)} - \frac{e^{-r/\delta_{eR}} + \Delta e^{-r/\delta_{iR}}}{2\left(1+\Delta\right)}, \tag{A5}$$

$$\Psi_{\alpha\alpha}\left(r\right) = 1 - \left(1 + \frac{r}{2\delta_{\alpha R}}\right)e^{-r/\delta_{\alpha R}}. \tag{A6}$$

Here $\Delta = \delta_{iR}/\delta_{eR}$. In this case Eq. (A3) yields

$$\begin{aligned}\left\langle E^2\right\rangle &= 2\pi n_e e_F^2\left(\frac{1}{\delta_{eR}} + \frac{Z}{\delta_{iR}}\right) \\ &+16\pi^2 n_e^2 e_F^2\left\{\sum_\alpha \int_0^\infty \left[g_{\alpha\alpha}\left(r\right) - 1\right]\Psi_{\alpha\alpha}\left(r\right) r dr - 2\int_0^\infty \left[g_{ei}\left(r\right) - 1\right]\Psi_{ei}\left(r\right) r dr\right\},\end{aligned} \tag{A7}$$

where $\Psi_{\alpha\alpha}(r)$ and $\Psi_{ei}(r)$ are now given by Eqs. (A5) and (A6). The first term in Eq. (A7) is precisely the second moment of the Holtsmark distribution obtained in Ref. [16] for the regularized interactions which is independent on Z_R. The second term arises due to correlations between particles. For the Coulomb interaction between plasma particles and the radiator with $\delta_{eR} \simeq 0$ or $\delta_{iR} \simeq 0$ the first term in Eq. (A7) diverges and the second moment of the MFD does not exist in this case.

---

[1] H. R. Griem, *Principles of Plasma Spectroscopy* (Cambridge University Press, Cambridge, 1997).
[2] D. Salzmann, *Atomic Physics in Hot Plasmas* (Oxford University Press, Oxford, 1998).
[3] J. Holtsmark, Ann. Phys. (Leipzig) **58**, 577 (1919).
[4] J. E. Mayer and M. G. Mayer, *Statistical Mechanics* (Wiley, New York, 1940).
[5] M. Baranger and B. Mozer, Phys. Rev. **115**, 521 (1959).
[6] B. Mozer and M. Baranger, Phys. Rev. **118**, 626 (1960).
[7] C. F. Hooper, Jr., Phys. Rev. **149**, 77 (1966).
[8] C. F. Hooper, Jr., Phys. Rev. **165**, 215 (1968).
[9] C. A. Iglesias, J. L. Lebowitz, and D. MacGowan, Phys. Rev. A **28**, 1667 (1983).
[10] A. Alastuey, C. A. Iglesias, J. L. Lebowitz, and D. Levesque, Phys. Rev. A **30**, 2537 (1984).
[11] J. W. Dufty, D. B. Boercker, and C. A. Iglesias, Phys. Rev. A **31**, 1681 (1985).
[12] M. Yu. Romanovsky and W. Ebeling, Contrib. Plasma Phys. **46**, 195 (2006).
[13] X.-Z. Yan and S. Ichimaru, Phys. Rev. A **34**, 2167 (1986).
[14] J. Ortner, I. Valuev, and W. Ebeling, Contrib. Plasma Phys. **40**, 555 (2000).
[15] B. Talin, A. Calisti, and J. Dufty, Phys. Rev. E **65**, 056406 (2002); B. Talin and J. Dufty, Contrib. Plasma Phys. **41**, 195 (2001).
[16] H. B. Nersisyan, C. Toepffer, and G. Zwicknagel, Phys. Rev. E **72**, 036403 (2005).
[17] H. B. Nersisyan and G. Zwicknagel, J. Phys. A **39**, 4677 (2006).
[18] T. Morita, Prog. Theor. Phys. **22**, 757 (1959); **23**, 1211 (1960).
[19] G. Kelbg, Ann. Phys. (Leipzig) **12**, 219 (1963); **13**, 354 (1964); **14**, 394 (1964).
[20] C. Deutsch, Y. Furutani, and M. M. Gombert, Phys. Rep. **69**, 85 (1981); C. Deutsch, Phys. Lett. A **60**, 317 (1977); C. Deutsch, M.-M. Gombert, and H. Minoo, *ibid.* **66**, 381 (1978); H. Minoo, M.-M. Gombert, and C. Deutsch, Phys. Rev. A **23**, 924 (1981).
[21] A. Munster, *Statistical Thermodynamics* (Springer, Berlin, 1969), vol. 1, Appendix 7.
[22] B. Held and C. Deutsch, Phys. Rev. A **24**, 540 (1981).
[23] A. Davletov and M.-M. Gombert, Phys. Rev. E **70**, 046404 (2004).
[24] C. de Dominicis and P. Martin, J. Math. Phys. **5**, 14 (1964).
[25] J.-P. Hansen and I. R. McDonald, *Theory of Simple Liquids* (Academic, New York, 1976).
[26] M. Baus and J. P. Hansen, Phys. Rep. **59**, 1 (1980).
[27] R. W. Zwanzig, J. Chem. Phys. **22**, 1420 (1954).
[28] I. S. Gradshteyn and I. M. Ryzhik, *Table of Integrals, Series and Products* (Academic, New York, 1980).
[29] T. Reed and K. Gubbins, *Applied Statistical Mechanics* (McGraw-Hill, New York, 1973).
[30] W. H. Press, B. P. Flannery, S. A. Teukolsky, and W. T. Vetterling, *Numerical Recipes* (Cambridge University Press, Cambridge, 1989).
[31] T. Pschiwul and G. Zwicknagel, Contrib. Plasma Phys. **41**, 217 (2001).
[32] A. Selchow, G. Röpke, A. Wierling, H. Reinholz, T. Pschiwul and G. Zwicknagel, Phys. Rev. E **64**, 056410 (2001).
[33] T. Pschiwul and G. Zwicknagel, J. Phys. A **36**, 6251 (2003).
[34] G. Zwicknagel and T. Pschiwul, Contrib. Plasma Phys. **43**, 393 (2003).
[35] I. Morozov, H. Reinholz, G. Röpke, A. Wierling, G. Zwicknagel, Phys. Rev. E **71**, 066408 (2005).
[36] G. Zwicknagel and T. Pschiwul, J. Phys. A **39**, 4359 (2006).
[37] J. Marten and C. Toepffer, Eur. Phys. J. D **29**, 397 (2004).
[38] A. Calisti, T. del Río Gaztelurrutia, B. Talin, High Energy Density Phys. **3**, 52 (2007).